

# Dual-channel quantum meta-hologram for display

Yubin Fan<sup>Ⓞ, a,b,c,†</sup> Hong Liang<sup>Ⓞ, d,e,†</sup> Yuhan Wang,<sup>†</sup> Shufan Chen,<sup>a,b,c</sup> Fangxing Lai,<sup>†</sup> Mu Ku Chen,<sup>a,b,c</sup> Shumin Xiao,<sup>†,g,\*</sup> Jensen Li,<sup>d,e,\*</sup> and Din Ping Tsai<sup>Ⓞ, a,b,c,\*</sup>

<sup>a</sup>City University of Hong Kong, Department of Electrical Engineering, Hong Kong, China

<sup>b</sup>City University of Hong Kong, Centre for Biosystems, Neuroscience, and Nanotechnology, Hong Kong, China

<sup>c</sup>City University of Hong Kong, The State Key Laboratory of Terahertz and Millimeter Waves, Hong Kong, China

<sup>d</sup>The Hong Kong University of Science and Technology, Department of Physics, Hong Kong, China

<sup>e</sup>The Hong Kong University of Science and Technology, IAS Center for Quantum Technologies, Hong Kong, China

<sup>f</sup>Harbin Institute of Technology (Shenzhen), Ministry of Industry and Information Technology Key Lab of Micro-Nano Optoelectronic Information System, Guangdong Provincial Key Laboratory of Semiconductor Optoelectronic Materials and Intelligent Photonic Systems, Shenzhen, China

<sup>g</sup>Pengcheng Laboratory, Shenzhen, China

**Abstract.** Quantum technologies rely on creating and manipulating entangled sources, which are essential for quantum information, communication, and imaging. By integrating quantum technologies and all-dielectric metasurfaces, the performance of miniature display devices can be enhanced to a higher level. Miniature display technology, such as virtual reality display, has achieved original commercial success, and was initially applied to immersive games and interactive scenes. While the consumer market has quickly adopted this technology, several areas remain for improvement, including concerns around bulkiness, dual-channel display, and noise reduction. Here, we experimentally realize a quantum meta-hologram concept demonstration of a miniature display. We fabricate an ultracompact meta-hologram based on 1  $\mu\text{m}$  thick titanium dioxide ( $\text{TiO}_2$ ). The meta-hologram can be remotely switched with heralding technique and is robust against noise with the quantum entangled source. The platform can alter the miniature display channel by manipulating heralding photons' polarization, removing speckles and multiple reflective light noise, improving imaging contrast, and potentially decreasing device weight. Imaging contrast increases from 0.36 dB under speckle noise influences to 6.8 dB in quantum correlation imaging. This approach has the potential to miniaturize quantum displays and quantum communication devices.

Keywords: quantum; meta-hologram; display; metasurface; dual channel.

Received Dec. 11, 2023; accepted for publication Dec. 21, 2023; published online Jan. 19, 2024.

© The Authors. Published by SPIE and CLP under a Creative Commons Attribution 4.0 International License. Distribution or reproduction of this work in whole or in part requires full attribution of the original publication, including its DOI.

[DOI: [10.1117/1.APN.3.1.016011](https://doi.org/10.1117/1.APN.3.1.016011)]

## 1 Introduction

The core technical trend of quantum technology is to exploit quantum phenomena such as entanglement for various applications. This trend has led to significant breakthroughs in precision measurement, computation, communication, and imaging. For example, entanglement is the primary quantum resource for breaking classical measurement limits.<sup>1</sup> Quantum communication provides an absolute security channel to protect national security and personal privacy. The entanglement-based Micius satellite secures quantum cryptography over 1120 km, even if

the satellite is manipulated.<sup>2</sup> The development of quantum technology has dramatically changed and will continue changing our way of life.

In future daily life, miniature display technology, such as virtual reality (VR), has the greatest potential to become the interface to the metaverse for human–digital interactions. The main technical path of VR devices like Fresnel lenses compresses the optical element thickness, which we call “miniature display devices.” Nevertheless, the size of the whole VR device is somewhat bulky because of its focal length. Pancake optics significantly reduces device size compared with Fresnel lenses, as it fully uses optical components for the light propagation space.<sup>3</sup> Recently, researchers from NVIDIA proposed a wearable binocular prototype that delivers a 3D full-color

\*Address all correspondence to Shumin Xiao, [shumin.xiao@hit.edu.cn](mailto:shumin.xiao@hit.edu.cn); Jensen Li, [jensenli@ust.hk](mailto:jensenli@ust.hk); Din Ping Tsai, [dptsai@cityu.edu.hk](mailto:dptsai@cityu.edu.hk)

<sup>†</sup>These authors contributed equally to this work

holographic near-eye display based on a geometric phase lens in one polarization channel. This innovative prototype dramatically reduces the weight of miniature display devices down to 60 g,<sup>4</sup> which shows a significant improvement in the weight of VR equipment. Currently, such display technology can be improved by adopting metasurfaces to become more compact. By going to a quantum source, it will further open up the possibility for miniature components for quantum communications with holographic capacity in storing/transmitting information in a high dimensional way as a “quantum display” of information. Users of miniature display devices also need to protect their privacy, including their viewing habits and biometric data. Thus the polarization multiplexed channel display is an excellent choice. A quantum meta-hologram display solution can provide a dual-channel display while potentially reducing weight.

Metasurfaces are a kind of high-performance platform composed of a subwavelength antenna. They are compact and friendly in integration.<sup>5–12</sup> Meta-holograms have been widely developed<sup>13–21</sup> under the rising tide of metasurfaces. They can reach high efficiency and provide vivid displays, especially after combining them with quantum correlation imaging.<sup>22–26</sup> Quantum correlation imaging is based on measuring photon correlations. An optical edge detection correlation imaging has been realized by a high-efficiency dielectric metasurface.<sup>25</sup> The apparent advantage of quantum correlation imaging is suppressing classical noise based on an entangled source.<sup>27</sup> At the same time, it is possible to remove the polarizer in the display terminal for quantum correlation imaging. After processing a coinciding measurement on its polarization-entangled sister photon, the star and triangle pattern is viewed individually on a metasurface.<sup>24</sup> A metasurface hologram using a heralded quantum source has been demonstrated.<sup>28</sup> Here, using a polarization-entangled photon pair, one more degree of freedom, the polarization of the heralding photon, can be utilized as a remote control for the hologram of the signal photon to display.

Here, we experimentally demonstrate a quantum meta-hologram concept demonstration of a miniature display platform. The platform can provide a dual-channel display, eliminate noise, improve imaging contrast, and potentially decrease device weight. We fabricate a high-efficiency polarization dependence hologram based on titanium dioxide (TiO<sub>2</sub>) and show outstanding noise suppression in display concept demonstration. Imaging contrast increases from 0.36 dB under the influence of speckle noise to 6.8 dB in quantum correlation imaging. The platform demonstrates the ability to remove multiple reflective lights, which is a shortcoming of the current miniature display devices. Our route will offer a novel function to the current miniature display devices and a new application area of quantum technology.

## 2 Results

### 2.1 Working Principle and Numerical Simulations

Polarization-entangled photon pairs in a pure state  $|\varphi\rangle = 1/\sqrt{2}(|H_h V_s\rangle + |V_h H_s\rangle)$  can be generated from spontaneous parametric downconversion (SPDC) using a type-II barium borate (BBO) crystal.<sup>29</sup> The subscripts in the formulas “*h*” and “*s*” throughout the paper are the first letters of “heralding” and “signal,” which are used to distinguish the photons in the heralding arm and the signal arm. Note that we use a half-wave plate (HWP) to correct the polarization rotation of the signal

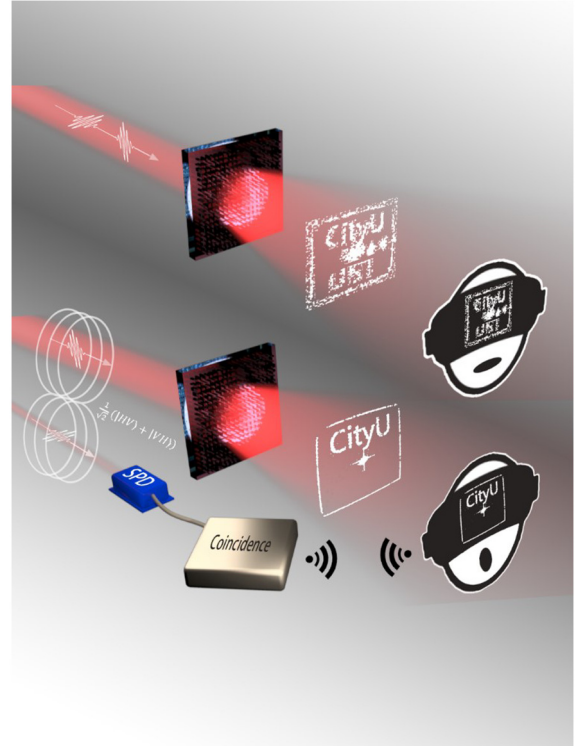


**Fig. 1** Schematic of quantum heralding meta-holograms of eliminating noise.

photons during transmission within the long fiber. After HWP, the state becomes  $|\varphi\rangle = 1/\sqrt{2}(|H_h V_s\rangle - |V_h H_s\rangle)$ . Interacting with the metasurface, the signal photons in horizontal (*H*) or vertical (*V*) polarizations are effectively correlated with the corresponding H-hologram  $|H, \text{CityU}\rangle$  or V-hologram  $|V, \text{UST}\rangle$  generated through the metasurface (the two holographic images in Fig. 1). The meta-holographic metasurface works as an operator  $\hat{M}_s = |V, \text{UST}\rangle\langle V| + |H, \text{CityU}\rangle\langle H|$ . The transformation of the polarization-entangled photon state can be summarized as

$$|\psi\rangle = (\hat{I}_h \otimes \hat{M}_s)|\varphi\rangle = \frac{1}{\sqrt{2}}(|H\rangle_h |V, \text{UST}\rangle_s - |V\rangle_h |H, \text{CityU}\rangle_s), \quad (1)$$

where the first (second) slot indicates the heralding (signal) photon, and we also define the density matrix  $\hat{\rho} = |\varphi\rangle\langle\varphi|$ . The herald photon polarizer operator is expressed as  $\hat{P}_h(\theta) = |\varphi_P\rangle\langle\varphi_P|$ , where  $|\varphi_P\rangle = \sin(\theta)|H\rangle + \cos(\theta)|V\rangle$ . After the polarized detection of the herald photon, the quantum state of the signal photon collapses into

$$\rho_s(\theta) = \text{Tr}_h\{\hat{P}_h(\theta) \otimes \hat{M}_s \hat{\rho} [\hat{P}_h(\theta) \otimes \hat{M}_s]^\dagger\}. \quad (2)$$

Thus, the signal photons show up in the designed holographic display by controlling the herald photon polarizer for  $\theta = 0$  and  $\theta = \pi/2$ ,

$$\begin{aligned}\rho_s(0) &= \text{Tr}_h\{[\hat{P}_h(0) \otimes \hat{M}_s]\rho[\hat{P}_h(0) \otimes \hat{M}_s]^\dagger\} \\ &= \frac{1}{2}|H, \text{CityU}\rangle_s\langle H, \text{CityU}|_s,\end{aligned}\quad (3)$$

$$\begin{aligned}\rho_s\left(\frac{\pi}{2}\right) &= \text{Tr}_h\{[\hat{P}_h(\pi/2) \otimes \hat{M}_s]\rho[\hat{P}_h(\pi/2) \otimes \hat{M}_s]^\dagger\} \\ &= \frac{1}{2}|V, \text{UST}\rangle_s\langle V, \text{UST}|_s.\end{aligned}\quad (4)$$

Note that only the desired polarization holographic display will show in this display prototype. The herald photon polarizer operator is positioned at  $\theta = 0$ ; the hologram  $|\text{CityU}\rangle$  displays in  $|H\rangle$  polarization; while the herald photon polarizer operator is positioned at  $\theta = \pi/2$ , the hologram  $|\text{UST}\rangle$  displays in  $|V\rangle$  polarization.

The working principle above provides an approach to realize a high-quality holographic display with low noise. It can improve the current display technologies, including diffractive optical elements-based Fresnel type, pancake type, and holographic glass display. However, those methods have bulky and heavy configurations. The Fresnel-type display has a thickness of several centimeters, at a minimum equal to the focal length of the display lens. The holographic glass achieves a thickness of only 2.5 mm.<sup>4</sup> The all-dielectric metasurfaces have the potential to overcome the mentioned difficulties through their advantages, such as thinness, low loss, and subwavelength structure size.

Titanium dioxide ( $\text{TiO}_2$ ) has been widely used in designing and fabricating metasurfaces in the visible range due to its excellent material features: high refractive index and low extinction coefficient. These superior characteristics make  $\text{TiO}_2$  a

superb candidate for display devices, providing huge phase modulation amplitude or high transmission. Figure 2(a) shows the phase of meta-hologram units at wavelengths of 810 nm. Figure 2(b) presents the simulation intensity of transmission varies with the size of the meta-hologram unit under an  $H$  polarization light incident with wavelengths of 810 nm. The phase and transmission resonance in  $V$  polarization becomes symmetrical by swapping width ( $w$ ) and depth ( $d$ ) axes. The label “ $w/l$ ” in the horizontal axis label denotes the ratio of width ( $w$ ) to length ( $l$ ), whereas the label “ $d/l$ ” in the vertical axis label represents the ratio of depth ( $d$ ) to length ( $l$ ). The detailed meta-hologram unit’s phase and transmittance are discussed in the [Appendix](#) and Note 1.1 in the [Supplementary Material](#). The thickness of  $\text{TiO}_2$  ( $h$ ) is fixed as 1  $\mu\text{m}$ , and its unit period ( $l$ ) is 500 nm, while  $w$  and  $d$  range from 100 to 450 nm with 10 nm intervals, as shown in the inset of Fig. 2(c). Changing the unit size will adjust the effective refractive index for specific dimensions, adding an additional phase for passing light. We can use two-dimensional (2D) units for two linear polarization holographic displays. The metaholographic displays consist of hologram images excited by  $H$  polarization ( $H$ -hologram) and  $V$  polarization ( $V$ -hologram). We changed the unit width to match the phase needs of the  $H$ -hologram and changed the depth for the  $V$ -hologram. The phase distribution and meta-hologram unit arrangement for both polarized holograms must match both phase requirements and ensure transmission efficiency. We use the Gerchberg–Saxton algorithm<sup>17,19</sup> to generate a metaholographic phase profile. Since two channels must be realized in a set of structural units, we select two polarized phases by minimizing phase differences, as shown in Note 1.1 in the [Supplementary Material](#). The units with transmission under 90% are all excluded while mapping. Black points in Figs. 2(a) and 2(b) are the final scales used in the metaholographic mapping.

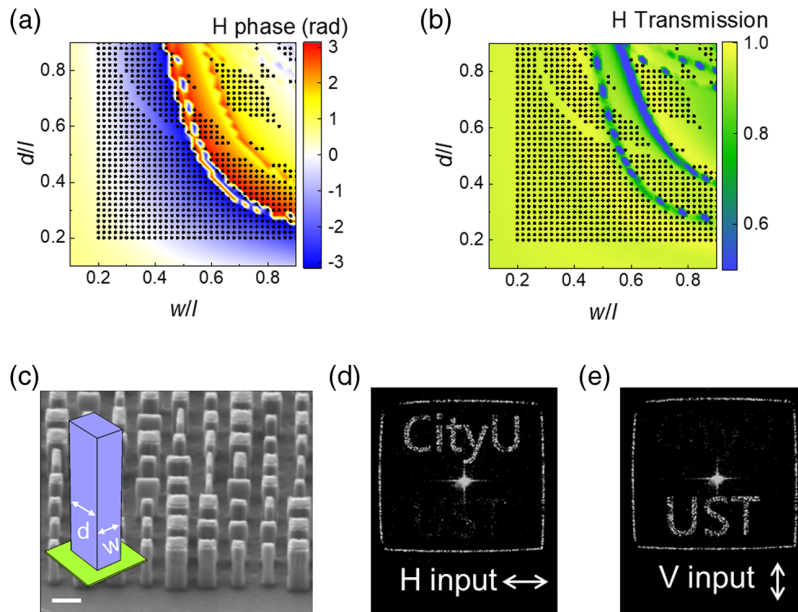


**Fig. 2** Design of metasurfaces and the classical holograms. (a) Unit phase and (b) transmission of  $H$  polarization for (c) metaholographic samples under an optical microscope; inset shows the unit cell, and scale bar is 500 nm. Black points in panels (a) and (b) are the final scales used in the metaholographic mapping. Metaholographic gray-scale image from (d) horizontal polarization and (e) vertical polarization by a gray-scale CCD camera.

## 2.2 Experimental Results

Based on the working principle and numerical simulations, we fabricated meta-holograms by the standard top-down complementary metal-oxide semiconductor process with  $100\ \mu\text{m} \times 100\ \mu\text{m}$  area and only  $1\ \mu\text{m}$  thickness for one meta-hologram. The metasurface can be directly fabricated on a glass substrate and significantly reduce the thickness of the miniature display device. The fabrication process is similar to previous work,<sup>30,31</sup> as seen in the [Appendix](#) and Note 1.2 in the [Supplementary Material](#). We measured two polarized meta-holographic images in a classical display prototype. The setup mainly includes a beam reduction part and a back focal plane (BFP) imaging part. The beam reduction part decreases the spot size of the classical incident linear polarized beam (810 nm from FIU-6, NKT Photonics), smaller than the metasurface sample size. The shaping of the incident light helps maximize the phase modulation of the incident light by the fabricated meta-hologram. After modulating by metasurface, the incident light dramatically spread and display the designed hologram. As the display spread angle is large, we use the BFP imaging technology to show the image indirectly. An objective lens with a large numerical aperture ( $\text{NA} = 0.8$ ) is involved and works for the Fourier transform of the metaholographic sample. A pair of lenses is used to build a  $4f$  imaging system for collecting the display image from the BFP of the objective lens ([Appendix](#) and Note 2 in the [Supplementary Material](#)). Note that the BFP imaging part is only used for demonstration, not necessarily in the final wearable device. The display results are shown in Figs. 2(d) and 2(e); the H-hologram |CityU) and V-hologram |UST) float while adjusting an HWP before the beam reduction. Three groups of metaholographic samples were fabricated. All holographic efficiencies are higher than 89% experimentally (Note 3.2 in the [Supplementary Material](#)). We select one of them to continue with the demo. The field of view (FoV) and eye box of this meta-hologram differ from those of the classical display platform we discussed in Note 3.4 in the [Supplementary Material](#).

With the polarization-dependent holograms confirmed by classical light, we now move on to the quantum optical imaging of the metasurface using entangled photon pairs. This part will show the ability to alter the display channel by manipulating the polarization of heralding photons. Figure 3(a) shows the experimental setup for obtaining the heralded holograms. Note that no polarizer is needed in the imaging (signal) arm, which shows the potential to further decrease the thickness and weight of miniature display devices. Pairs of polarization-entangled photons of vertical ( $V$ ) and horizontal ( $H$ ) polarizations at 810 nm are generated by SPDC with a BBO crystal, as shown in the left dashed box in Fig. 3(a). One photon is sent through the signal arm [upper light path in Fig. 3(a)], while another is sent through the heralding arm [lower light path in Fig. 3(a)] with a linear polarizer for selecting the heralding polarization. The two photons travel through fibers, one to a single-photon counting module to herald the arrival of a photon at the single-photon avalanche diode (SPAD) camera, while another is sent to the meta-hologram, and the SPAD camera images the far-field hologram image. The HWP before the meta-hologram is used to correct the small polarization rotation due to the light traveling through the long fiber. When the heralding mechanism is turned on with the SPAD camera, a 10 ns time window of the current frame is used to register photon arrival events in the signal arm whenever a photon is registered in the heralding arm. When the

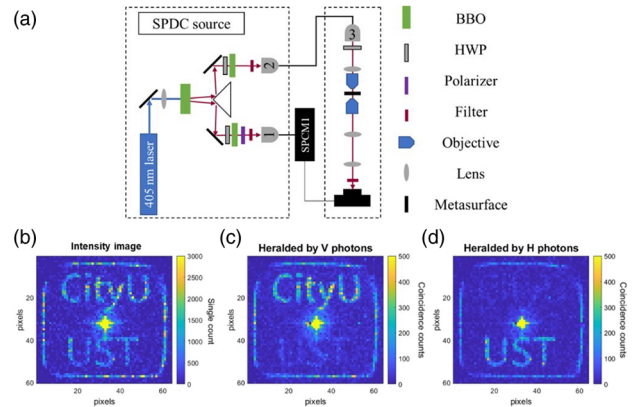


**Fig. 3** Experimental setup for obtaining heralded holograms on metasurface. (b) Intensity image of hologram obtained with single photons without heralding. (c) Hologram with heralding photons of vertical polarization. (d) Hologram with heralding photons of horizontal polarization. All images are obtained with 6000 100-ms-long 8-bit frames, and the background is subtracted.

heralding mechanism is turned off, photons arriving at any time are registered.

The hologram generated without heralding signals is imaged in a total of 6000 frames and is shown in Fig. 3(b). Each frame spans 100 ms, with a maximum of 255 photons per pixel registered in a single frame. The pixels of letters “CityU” (“UST”) show an average of 1089 (723) photons per pixel and a contrast of 9.8 (8.0) dB above the background of 115 photon counts (Note 3 in the [Supplementary Material](#)). Without heralding, the hologram captures responses from both  $V$  and  $H$  polarizations, independent of the setting of the polarizer in the heralding arm. We set the linear polarizer to select  $V$  polarization with the heralding mechanism turned on. The hologram is displayed in Fig. 3(c), clearly showing up only the letters “CityU,” which is generated by  $H$ -polarization photons. On the other hand, when the linear polarizer is switched to  $H$  polarization, the hologram imaged shows “UST,” the hologram generated by  $V$ -polarization. Our use of polarization-entangled resources is the primary advantage, leveraging the correlation of single-photon pairs. This allows us to achieve dual-channel display together with remote control capabilities.

To denote the quality of the heralded holograms, we choose the signal-to-noise ratio (SNR) and Pearson correlation coefficient to compare the experimental holograms with the designed ones, which can contain only “CityU” or “UST” or both letters. In both holograms in Figs. 3(c) and 3(d), the SNRs and Pearson correlation coefficients achieved are both 4.4 dB and 0.80, indicating distinguishable hologram signals. We note that an outer frame encloses both holograms, originally designed in both  $V$ - and  $H$ -holograms. In comparison, the hologram imaged without heralding photons [Fig. 3(b)] has an SNR (Pearson correlation coefficient) of 3.1 dB (0.73), which is lower than that of the heralded holograms. Background noise can also be effectively reduced by pulsed-light-gated cameras. They do not guarantee to display in two independent polarization channels. Fortunately, our heralding holograms offer a unique advantage in the form of polarization correlation, which enables us to select between two polarization channels. With the ability to remotely select between two channels and achieve polarization display channel selection simultaneously, we are

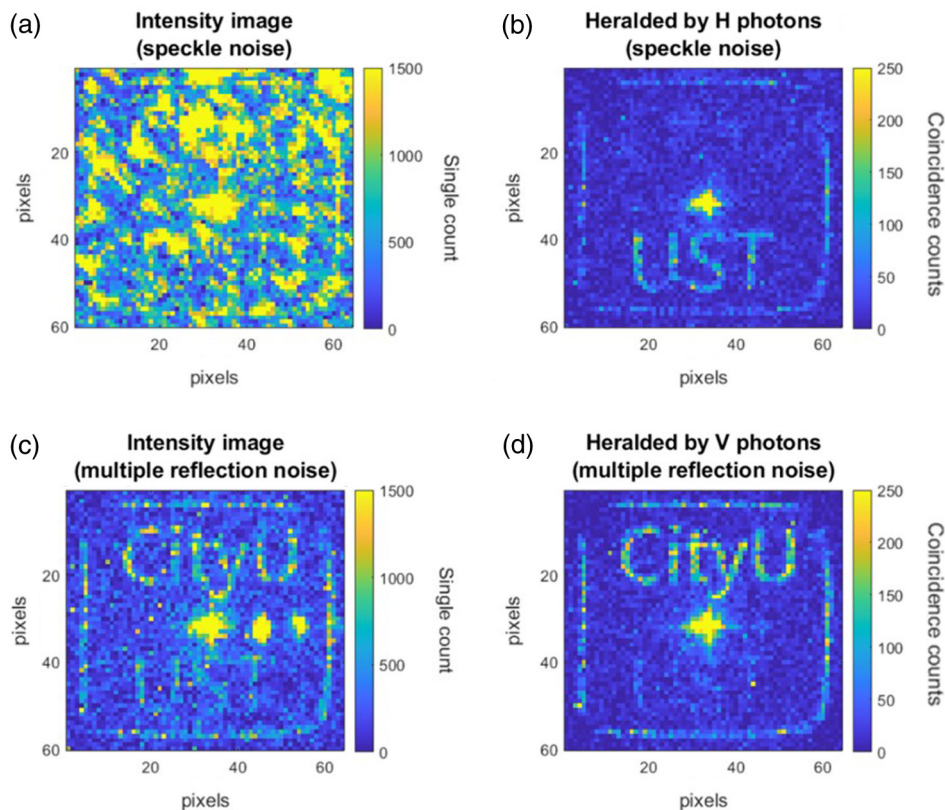


**Fig. 4** (a) Intensity hologram under an additional illumination as noise background. (b) Hologram with heralding photons of horizontal polarization in the same situation. (c) Metaholographic display influenced by multiple reflective lights. (d) Multiple reflective lights are suppressed significantly after quantum correlation imaging.

breaking new ground and unlocking new realms of possibility for imaging and display technology.

An advantage of using the heralding mechanism in generating polarization-multiplexed holograms lies in its robustness against noisy environments. We demonstrate this aspect by experimenting with additional illumination as a noisy background. Figure 4(a) shows the intensity image of the hologram without heralding obtained by the SPAD camera. In this case, the photon number in the background has an average of 837 per pixel and a standard deviation of 690 with a total of 6000 frames, and the hologram is of low contrast. The pixels of letters “CityU” (“UST”) show an average of 1666 (908) photons per pixel and a contrast of 3.0 (0.36) dB. Effective information is submerged in speckle noise, rendering it indistinguishable in the display. The SNR dropped from 3.1 dB in Fig. 3(b) to 1.3 dB (0.73 to 0.35 for Pearson correlation coefficient) in Fig. 4(a). On the other hand, for the hologram with horizontal heralding photons, as shown in Fig. 4(b), the H-hologram “UST” can still be clearly seen with a high contrast of 6.8 dB, effectively improved from 0.36 dB under the influence of speckle noise, and the SNR slightly dropped from 4.4 to 2.4 dB (0.80 to 0.62 for Pearson correlation coefficient), which is due to the attenuated signals because of the beam splitter and the accidental arrival of some background photons within the 10 ns heralding detection window.

To further show the potential application in multiple display cases, we also demonstrate suppressing multiple reflective lights from surfaces of optical elements.<sup>32,33</sup> Here, correlation imaging

is used to suppress the influence of multiple reflective lights with additional illumination. We generate multiple reflective lights with a pair of face-to-face 50:50 beam splitters (Note 2.3 in the [Supplementary Material](#)). The multiple reflective lights influence is shown in Fig. 4(c). Two weaker residual light spots from multiple reflections appear on the right side of the normal incident light. After heralding, the multiple reflective light spots are visibly removed in Fig. 4(d). While our current quantum meta-hologram-based display platform concept demonstration is limited to displaying two static images of entangled polarization, the combination of spatial light modulator and our quantum meta-hologram are aimed at delving deeper into programmable demonstrations in the future. Although the quantum light source is very weak for the human eye under the current situation, stronger quantum light sources are still in development. In fact, several ongoing research efforts are to enhance the performance of quantum light sources, such as using a metalens array,<sup>21</sup> a resonance metasurface,<sup>34</sup> and 2D materials.<sup>35</sup> We believe our method can benefit from these advances and provide a novel way of achieving high-quality holographic displays.

### 3 Discussion and Conclusion

In summary, we presented a quantum meta-hologram-based display platform concept demonstration of miniature display devices. The  $\text{TiO}_2$  meta-hologram in quantum correlation imaging shows outstanding robustness against noisy environments with ultracompact size in the holographic display process. Imaging

contrast increases from 0.36 dB in classical imaging under the influence of speckle noise to 6.8 dB in quantum correlation imaging, quantitatively denoting the quality of the quantum heralding holographic display in two polarization channels. The conceptual platform also demonstrates the ability to eliminate speckle noise and multiple reflective light noises. Furthermore, the possibility of improving the demonstrated quantum display device, allowing additional remote control of the information to be displayed through heralding techniques, is mentioned. This work presents an ultracompact, friendly, integrated, dual-channel display and noise elimination display platform concept by combining meta-hologram and quantum correlation imaging. Our route will offer a novel function to the current miniature display devices and a new application area of quantum technology.

## 4 Appendix: Online Methods

### 4.1 Sample Fabrication

The manufacturing process is summarized in Fig. S3 in the [Supplementary Material](#). First, the 1  $\mu\text{m}$   $\text{TiO}_2$  film, deposited on 13 nm ITO, coated with 200 nm photoresist [PMMA A2] is patterned by electron beam lithography (Raith Eline 150Plus). After irradiation, the samples are developed in the developer solution (MIBK/IPA with a ratio of 1:3) for 30 s. To obtain a high selection ratio, Cr film is selected as the etching mask: 30 nm Cr film is deposited, then lifted off by remover PG. Finally, the  $\text{TiO}_2$  cuboid is formalized by the RIE dry-etching process (Oxford PlasmaPro 800).

### 4.2 Simulation and Holographic Design

The numerical calculation of the meta-hologram phase unit is designed by COMSOL Multiphysics. We swept the weight and depth of a unit and extracted the phase and transmission of the input linear polarized plane wave in the wavelength domain, as shown in Figs. 2(a) and 2(b). We directly flip the weight and depth, as the unit size is symmetrical for both linear polarizations. Until now, we have gotten the phase and transmission of the unit cell.

The next step is generating metaholographic phase mapping. We use the G-S algorithm to generate phase profiles for both polarizations separately. As two channels must be realized in a set of structural units, we select two polarized phases by minimizing phase differences. The units that transmittance less than 90% are all excluded while mapping. See Note 1 in the [Supplementary Material](#) for more details.

### 4.3 Measurement Setup

A classical imaging setup and a quantum correlation imaging system are built to characterize our meta-holograms. The classical imaging setup is composed of a beam reduction part and a BFP imaging part. The beam reduction part decreases the classical incident linear polarized beam (810 nm from FIU-6, NKT Photonics) and displays it in a CCD camera. Such a classical setup is also a part of the quantum correlation imaging system. We replace the CCD camera with a SPAD array camera in the quantum correlation imaging system. See Note 2 in the [Supplementary Material](#) for more details.

## Disclosures

The authors declare no competing financial interests.

## Code and Data Availability

The main data supporting the findings of this study are available within the article and its [Supplementary Material](#). All data generated in the present study are available from the corresponding author upon reasonable request. All simulation and data processing codes in the present study are available from the corresponding author upon reasonable request.

## Acknowledgments

This work was supported by the University Grants Committee/Research Grants Council of the Hong Kong Special Administrative Region, China (Grant No. AoE/P-502/20; CRF Project: C5031-22G and C1015-21E; and GRF Project: 15303521, 11310522, 11305223, 11300123, 16304020, and 16306521), the Department of Science and Technology of Guangdong Province (Grant No. 2020B1515120073), the City University of Hong Kong (Grant Nos. 9380131, 9610628, and 7005867), and the National Key R&D Program of China (Grant No. 2022YFA1404700). The authors thank Geyang Qu and Qinmiao Chen from the Harbin Institute of Technology for helpful discussions in metaholographic phase design.

## References

1. H. Strobel et al., “Fisher information and entanglement of non-Gaussian spin states,” *Science* **345**(6195), 424–427 (2014).
2. J. Yin et al., “Entanglement-based secure quantum cryptography over 1,120 kilometres,” *Nature* **582**(7813), 501–505 (2020).
3. J. Xiong et al., “Augmented reality and virtual reality displays: emerging technologies and future perspectives,” *Light: Sci. Appl.* **10**(1), 216 (2021).
4. J. Kim et al., “Holographic glasses for virtual reality,” in *ACM SIGGRAPH 2022 Conf. Proc.*, pp. 1–9 (2022).
5. Y. Fan et al., “Emerging trend in unconventional metasurfaces: from nonlinear, non-Hermitian to nonclassical metasurfaces,” *ACS Photonics* **9**(9), 2872–2890 (2022).
6. J. Yao et al., “Plasmonic anapole metamaterial for refractive index sensing,” *PhotonIX* **3**(1), 23 (2022).
7. M. K. Chen et al., “Artificial intelligence in meta-optics,” *Chem. Rev.* **122**(19), 15356–15413 (2022).
8. M. K. Chen et al., “A meta-device for intelligent depth perception,” *Adv. Mater.* **35**(34), 2107465 (2023).
9. W. C. Wong et al., “Quantum optics of lossy metasurfaces: propagating the photon-moment matrix by the semiclassical Liouvillian,” *Phys. Rev. A* **106**(1), 013503 (2022).
10. Y. Wang et al., “Highly controllable etchless perovskite microlasers based on bound states in the continuum,” *ACS Nano* **15**(4), 7386–7391 (2021).
11. M. K. Chen et al., “Meta-lens in the sky,” *IEEE Access* **10**, 46552–46557 (2022).
12. Y. Fan et al., “Enhanced multiphoton processes in perovskite metasurfaces,” *Nano Lett.* **21**(17), 7191–7197 (2021).
13. Q. Jiang, G. Jin, and L. Cao, “When metasurface meets hologram: principle and advances,” *Adv. Opt. Photonics* **11**(3), 518–576 (2019).
14. G. Zheng et al., “Metasurface holograms reaching 80% efficiency,” *Nat. Nanotechnol.* **10**(4), 308–312 (2015).
15. X. Li et al., “Multicolor 3D meta-holography by broadband plasmonic modulation,” *Sci. Adv.* **2**(11), e1601102 (2016).
16. W. Zhao et al., “Dielectric Huygens’ metasurface for high-efficiency hologram operating in transmission mode,” *Sci. Rep.* **6**(1), 30613 (2016).

17. Y. Gao et al., “Nonlinear holographic all-dielectric metasurfaces,” *Nano Lett.* **18**(12), 8054–8061 (2018).
18. Y.-W. Huang et al., “Aluminum plasmonic multicolor meta-hologram,” *Nano Lett.* **15**(5), 3122–3127 (2015).
19. W. T. Chen et al., “High-efficiency broadband meta-hologram with polarization-controlled dual images,” *Nano Lett.* **14**(1), 225–230 (2014).
20. G. Qu et al., “Reprogrammable meta-hologram for optical encryption,” *Nat. Commun.* **11**(1), 5484 (2020).
21. L. Li et al., “Metalens-array-based high-dimensional and multi-photon quantum source,” *Science* **368**(6498), 1487–1490 (2020).
22. T. K. Yung et al., “Polarization coincidence images from metasurfaces with HOM-type interference,” *iScience* **25**(4) (2022).
23. P.-A. Moreau et al., “Ghost imaging using optical correlations,” *Laser Photonics Rev.* **12**(1), 1700143 (2018).
24. C. Altuzarra et al., “Imaging of polarization-sensitive metasurfaces with quantum entanglement,” *Phys. Rev. A* **99**(2), 020101 (2019).
25. J. Zhou et al., “Metasurface enabled quantum edge detection,” *Sci. Adv.* **6**(51), eabc4385 (2020).
26. H. Defienne et al., “Pixel super-resolution with spatially entangled photons,” *Nat. Commun.* **13**(1), 3566 (2022).
27. H. Defienne et al., “Polarization entanglement-enabled quantum holography,” *Nat. Phys.* **17**(5), 591–597 (2021).
28. J.-Z. Yang et al., “Quantum metasurface holography,” *Photonics Res.* **10**(11), 2607–2613 (2022).
29. C. Couteau, “Spontaneous parametric down-conversion,” *Contemp. Phys.* **59**(3), 291–304 (2018).
30. J. Cheng et al., “Ultracompact orbital angular momentum sorter on a CMOS chip,” *Nano Lett.* **22**(10), 3993–3999 (2022).
31. X. Zhang et al., “Chiral emission from resonant metasurfaces,” *Science* **377**(6611), 1215–1218 (2022).
32. T. Okuno, “Development of subwavelength structure coating (SWC) and its application to imaging lenses,” in *Int. Opt. Des. Conf.*, Optica Publishing Group, p. IMA2 (2010).
33. T. Zhan et al., “Practical chromatic aberration correction in virtual reality displays enabled by cost-effective ultra-broadband liquid crystal polymer lenses,” *Adv. Opt. Mater.* **8**(2), 1901360 (2020).
34. T. Santiago-Cruz et al., “Resonant metasurfaces for generating complex quantum states,” *Science* **377**(6609), 991–995 (2022).
35. Q. Guo et al., “Ultrathin quantum light source with van Der Waals NbOCl<sub>2</sub> crystal,” *Nature* **613**(7942), 53–59 (2023).

Biographies of the authors are not available.